THE JOURNAL OF PHYSICAL CHEMISTRY B

Article

Cite This: J. Phys. Chem. B 2019, 123, 10410−10423

pubs.acs.org/JPCB

Reaction Kinetics, Product Branching, and Potential Energy Surfaces of $^1O_2$-Induced 9-Methylguanine−Lysine Cross-Linking: A Combined Mass Spectrometry, Spectroscopy, and Computational Study

Yan Sun,[†,‡] Midas Tsai,[§] Wenjing Zhou,[†] Wenchao Lu,[†,‡] and Jianbo Liu*[,†,‡]

[†]Department of Chemistry and Biochemistry, Queens College of the City University of New York, 65-30 Kissena Blvd., Queens, New York 11367, United States

[‡]Ph.D. Program in Chemistry, The Graduate Center of the City University of New York, 365 5th Avenue, New York, New York 10016, United States

[§]Department of Natural Sciences, LaGuardia Community College, 31-10 Thomson Avenue, Long Island City, New York 11101, United States

Supporting Information

ABSTRACT: We report a kinetics and mechanistic study on the $^1O_2$ oxidation of 9-methylguanine (9MG) and the cross-linking of the oxidized intermediate 2-amino-9-methyl-9*H*-purine-6,8-dione (9MOG^{OX}) with N^{α}-acetyl-lysine-methyl ester (abbreviated as LysNH$_2$) in aqueous solutions of different pH. Experimental measurements include the determination of product branching ratios and reaction kinetics using mass spectrometry and absorption spectroscopy, and the characterization of product structures by employing collision-induced dissociation. Strong pH dependence was revealed for both 9MG oxidation and the addition of nucleophiles (water and LysNH$_2$) at the C5 position of 9MOG^{OX}. The $^1O_2$ oxidation rate constant of 9MG was determined to be 3.6×10^7 M^{-1}·s^{-1} at pH 10.0 and 0.3×10^7 M^{-1}·s^{-1} at pH 7.0, both of which were measured in the presence of 15 mM LysNH$_2$. The ωB97XD density functional theory coupled with various basis sets and the SMD implicit solvation model was used to explore the reaction potential energy surfaces for the $^1O_2$ oxidation of 9MG and the formation of C5-water and C5-LysNH$_2$ adducts of 9MOG^{OX}. Computational results have shed light on reaction pathways and product structures for the different ionization states of the reactants. The present work has confirmed that the initial $^1O_2$ addition represents the rate-limiting step for the oxidative transformations of 9MG. All of the downstream steps are exothermic with respect to the starting reactants. The C5-cross-linking of 9MOG^{OX} with LysNH$_2$ significantly suppressed the formation of spiroiminodihydantoin (9MSp) resulting from the C5-water addition. The latter became dominant only at the low concentration (∼1 mM) of LysNH$_2$.

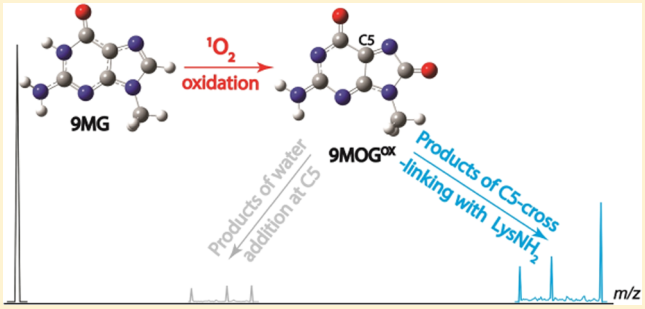

1. INTRODUCTION

Singlet $O_2[a^1\Delta_g]$[1] may induce nucleobase modifications, abasic sites, and strand breaks of DNA. Guanine presents the lowest oxidation potential[2,3] and the lowest ionization energy[4,5] among the four DNA nucleobases and thus is the most oxidizable base. The oxidation of guanine by $^1O_2$ has been investigated in various structural contexts including free nucleobases,[6−9] nucleosides,[10−16] base pairs,[17] single- and double-stranded DNA,[18] G-quadruplex DNA,[19] and isolated[18,20] and cellular DNA.[18,21] The experiments were conducted both in the gas phase[6−8,17] and in conventional condensed phase,[9−14,16,18,21] using different $^1O_2$-generation methods. Reaction kinetics, reaction dynamics, and structures of oxidation intermediates have been continuously revised with new experimental findings, augmented by theoretical explorations using electronic structure calculations[22−26] and molecular dynamics simulations.[27,28] A commonly accepted $^1O_2$ oxidation mechanism of guanosine (G) nucleoside is illustrated in Scheme 1.[29−33] G is attacked by $^1O_2$ on the imidazole ring, forming an endoperoxide via a [4 + 2] cycloaddition. The latter quickly converts to a hydroperoxide 8-OOHG. The fate of 8-OOHG depends on reaction conditions and structural contexts. The 8-OOHG within DNA is reduced to 8-oxo-7,8-dihydrodeoxyguanosine (OG) via Path 1, and OG reacts with a second $^1O_2$ to form a 5-hydroperoxy-8-oxo-7,8-dihydrodeoxyguanosine (5-OOH-OG) intermediate and eventually an oxidized form of 5-guanidinohydantoin (Gh^{OX});[30] free 8-OOHG or that contained in short oligonucleotides follows Path 2 instead and converts to a quinonoid intermediate 2-amino-9*H*-purine-6,8-dione (OG^{OX}).

One of the downstream reactions of OG^{OX} is rehydration to form 2-amino-5-hydroxy-7,9-dihydropurine-6,8-dione (5-OH-

Received: September 16, 2019
Revised: October 28, 2019
Published: November 13, 2019

DOI: 10.1021/acs.jpcb.9b08796
J. Phys. Chem. B 2019, 123, 10410−10423

Scheme 1. $^1O_2$ Oxidation of dGuo and Its Cross-Linking with $LysNH_2$[a]

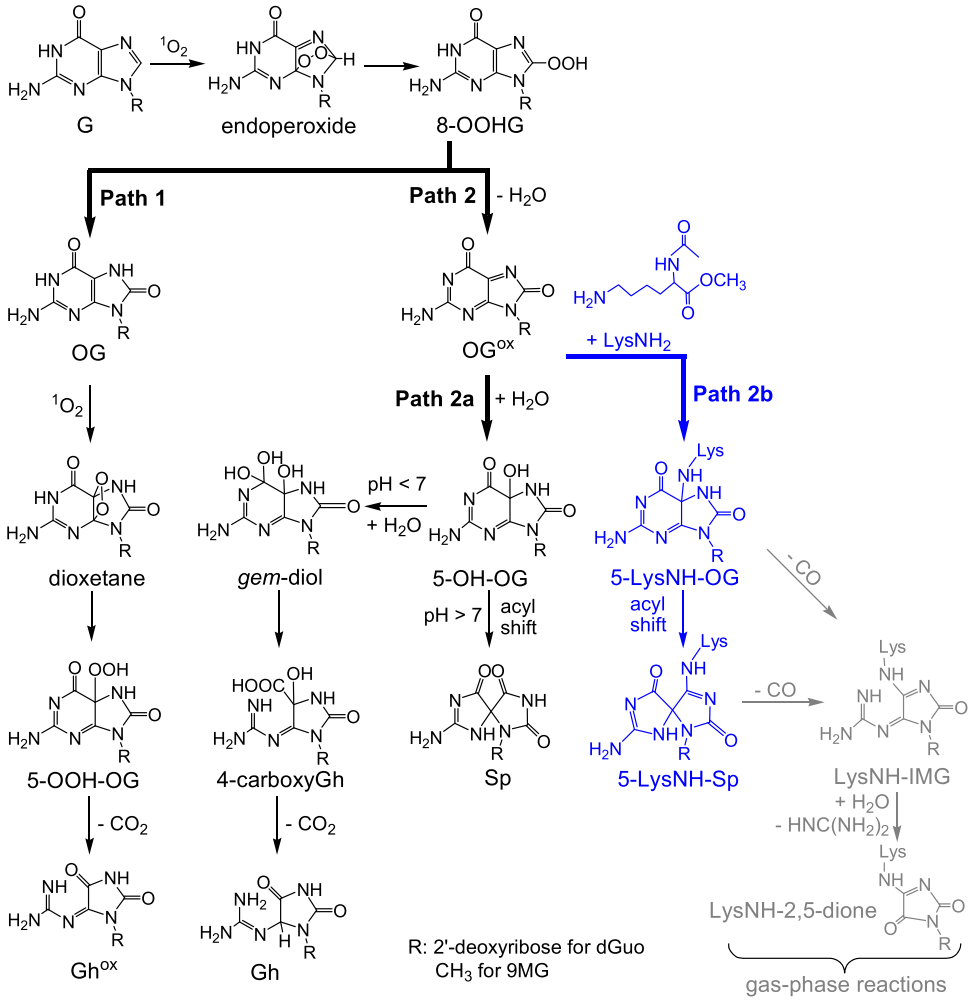

[a]The blue-colored pathway indicates the cross-linking process, while the gray-colored pathways show secondary reactions of 5-Lys-NH-OG and 5-Lys-NH-Sp in the gas phase.

OG, Path 2a). 5-OH-OG may convert to spiroiminodihydantoin (Sp) through an acyl shift under basic conditions[15] or 5-guanidinohydantoin (Gh) through the intermediacy of a *gem*-diol intermediate under acidic conditions.[13,22] Another OG^{OX}-mediated reaction is the covalent cross-linking with amino acid residues, referred to as DNA−protein cross-links (DPCs).[26,34,35] DPCs are of utmost importance in biology and must be repaired for cell survival as they may block transcription and replication.[34] On the other hand, DPCs are the least understood DNA lesion due to their various intermediate structures and formation mechanisms. DPCs may be mediated not only by OG^{OX} that follows the $^1O_2$ oxidation of guanine[26,34,35] but also by guanine radical cations (and its deprotonated species) that follow the one-electron oxidation of guanine.[35−40] Lysine has a large abundance in histones, one of the main protein components of eukaryotic chromatin.[36] The proximity of lysine to the guanine bases in DNA makes this amino acid of considerable interest in the oxidatively generated DPCs. Burrows and co-workers have examined the H_2O-, NH_3-, and lysine adducts of the oxidized guanine in nucleosides and single- and double-stranded oligodeoxynucleotides.[34,41] They reported different DPC structures depending on the nature of oxidants, e.g., $^1O_2$, lysine radicals, Na_2IrCl_6, or sulfate radicals. Accompanying the experimental work, Schlegel and co-workers have explored the $^1O_2$- and radical-mediated reaction pathways and intermediates for guanine−lysine cross-linking using various electronic structure calculations.[26,40,42] More recently, Dumont and co-workers have probed guanine−lysine cross-links using molecular dynamics simulations.[43,44] The $^1O_2$-specific guanine−lysine cross-linking mechanism may be summarized by Path 2b (highlighted in blue in Scheme 1). That is, the presence of lysine during the $^1O_2$ oxidation of G produces C5-lysine-substituted spiroiminodihydantion 5-LysNH-Sp exclusively.[26,34]

We have recently reported the $^1O_2$ oxidation kinetics of free guanine and 9-methylguanine (9MG) at different pH.[9] In that work, we measured the oxidation rate constants and product branching ratios of guanine and 9MG, determined the structures of their oxidation products, and explored their reaction potential energy surfaces (PESs). In the present study, we continued to elucidate the $^1O_2$ oxidation kinetics of 9MG in the presence of lysine as a competing nucleophile with water for C5-addition. The emphasis of our work was placed on quantitative measurements of cross-linking kinetics and branching ratios between the formation of Sp and C5-LysNH-Sp, and computational dissection of reaction mechanisms. In the current work, 9MG was used as a prototype

DOI: 10.1021/acs.jpcb.9b08796
J. Phys. Chem. B 2019, 123, 10410−10423

compound[45−49] to mimic guanine nucleoside. 9MG has the same protonation (N7) and deprotonation (N1) sites as guanosine. The pK_a values of 9MG are 3.11 (pK_{a1}) and 9.56 (pK_{a2}),[50] which are close to 2.20 and 9.50 for guanosine[51] and 2.30−2.85 and 9.99−10.18 for guanine bases in oligonucleotides.[52] Note that the ribose 2′,3′-diol deprotonates at pH > 12[51,53] and thus could not compete for deprotonation with guanine. N^{α}-acetyl-lysine-methyl ester (abbreviated as LysNH_2 in the remainder of this paper) was used as a model peptide to prevent the reactions of α-amino and carboxylate termini with 9MG.[34]

2. EXPERIMENTAL METHODOLOGIES

All chemicals were used without further purification. Reaction solutions containing 0.03 mM of 9MG (≥98%, Chemodex) and 15 mM of LysNH_2 (N^{α}-acetyl-L-lysine-methyl ester hydrochloride, 98%, Sigma-Aldrich) were prepared in pH 7.0 phosphate buffer (0.05 mM, Alfa Aesar) or pH 10.0 borax/NaOH buffer (MP Biomedicals). The UV absorbance of 9MG fell within the range of 0.6−1.0 to ensure a linear relationship between the absorbance and reactant concentration in the kinetics measurement. For mass spectrometric measurement, reaction solutions were prepared with 1.5 mM 9MG and 15 mM LysNH_2 at pH 7.0, and 2.5 mM 9MG and 15 mM LysNH_2 at pH 10.0, for which pH was adjusted using phosphate buffer or NaOH solution. The experimental setup was reported before,[9] and a schematic drawing is shown in Figure S1 in the Supporting Information. Only a brief description is given below.

$^1O_2$ was generated by the reaction of H_2O_2 + Cl_2 + 2KOH → $^1O_2/^3O_2$ + 2KCl + 2H_2O.[54,55] In the experiment, 10.5 mL of 8 M KOH was mixed with 20 mL of 35% H_2O_2 in a sparger (**1**, see Figure S1 in the Supporting Information) held at −17 °C. 4.4 sccm of Cl_2 and 96 sccm of He were mixed in a gas proportioner and bubbled through the H_2O_2/KOH slush. Cl_2 reacted with H_2O_2 completely to produce a mixture of $^1O_2$, $^3O_2$, and water. The water vapor was removed by passing the gas products through a −70 °C cold trap (**2**). The concentration of $^1O_2$ in the gas phase was determined by measuring $^1O_2$ emission ($a^1\Delta_g \rightarrow X^3\Sigma_g^-$)[56] at 1270 nm in an optical emission cell (**3**), where the collimated emission was transmitted through an optical chopper (**4**), detected by a cooled InGaAs detector (**5**), and processed by a lock-in amplifier. The gas mixture was then passed into a reaction vessel (**6**), which contained the solution of 9MG and LysNH_2. To achieve quasi-steady-state [$^1O_2$] in the solution (see the calibration of solution-phase [$^1O_2$] in the Supporting Information),[57] **6** was continuously evacuated by a mechanical pump (**7**) with its pressure maintained at 25 Torr using a pressure relay (**8**). To compensate for the loss of water by evaporation at the reduced pressure, the same amount of makeup solvent was replenished into **6** by a rotary piston pump (**9**).

The online monitoring system consisted of a UV−vis spectrometer (**10**), a fluorometer (**11**), and an electrospray ionization mass spectrometer (ESI MS, **13**−**16**). Reaction solution was circulating through the spectrometers using a peristaltic pump (**12**). In the present work, only UV−vis absorption was used in parallel with MS to monitor reaction progress since there was no fluorescence detected from 9MG under neutral and basic conditions. Absorption spectra were recorded every 10 s, and each spectrum was averaged over 25 scans. For ESI MS measurement, 150 μL of the reaction solution was loaded to the sampling loop of a two-position switching valve (**13**) and then inserted to the MS injection route. A theta-glass capillary (**14**) was used as an ESI emitter.[58−60] One channel of the theta capillary was used to transport the solution from the sampling loop using a syringe pump (**15a**, 0.01 mL/h), and the other channel was to deliver methanol using a second syringe pump (**15b**, 0.04 mL/h). Adding methanol to electrospray minimized the sample amount for MS analysis and avoided corona discharge[61] of the aqueous solution in the negative ion mode.

MS measurement was carried out on a homemade guided-ion-beam tandem mass spectrometer (**16**) described in detail before.[62] In regular MS measurement, ions were guided to the first quadrupole mass analyzer of the mass spectrometer for mass analysis, and the second quadrupole mass analyzer of the mass spectrometer was rendered to an ion guide mode, passing all of the ions to an electron multiplier detector. MS spectra were recorded at an interval of 60 s. In the CID MS/MS measurement, product ions of interest were selected by the first quadrupole mass filter and then collected into an octopole ion guide, which runs through a scattering cell filled with a 0.35 mTorr xenon gas (99.995%, Spectra Gases). CID was measured at the center-of-mass collision energy (E_{col}) of 1.5 eV. Fragment ions and the remaining primary ions were analyzed by the second quadrupole, and MS/MS fragmentation spectra were used to identify product ion structures and compared with the literature (if available) to confirm their assignments.

Experiments were conducted in triplicate, and their deviations were within 10%. The data presented are the averages of three data sets. On the basis of the comparison between UV−vis and MS-measured rate constants,[9] the overall uncertainties in rate constant (and product branching ratio) measurements are within 15%. $^1O_2$-specific products were distinguished by comparing with control experiments conducted using pure $^3O_2$, and none of these products were observed in the reactions with $^3O_2$.

3. COMPUTATIONAL DETAILS

Geometries of reactants, products, intermediates, and transition states (TSs) were optimized at the ωB97XD level of theory coupled with the 6-31+G(d,p)[63] basis set and the SMD solvation model.[64] ωB97XD[65] mitigates self-interaction errors and improves the orbital description of ionized states. All calculations were carried out using Gaussian 09 (revision D.01).[66] TSs were verified using frequency calculations and intrinsic reaction coordinate (IRC) evaluation. Cartesian coordinates for all of the calculated structures are provided in the Supporting Information. Reaction enthalpies and PESs were evaluated by the sum of electronic energies, zero-point energies (ZPEs), and thermal corrections at 298 K, of which the ZPEs were scaled by a factor of 0.975.[67]

As a first step in exploring reaction PESs, the conformations of 9MG and LysNH_2 had to be fully screened. The conformers of neutral, protonated, and deprotonated 9MG were reported in our previous work.[9] The lysine amino acid (i.e., H_2N−$C(CO_2H)$−$(CH_2)_4NH_2$) has eight degrees of rotational freedom. The full combinations of single-bond rotations resulted in a total of 17 496 possible canonical structures. Leng et al. conducted exhaustive searches among these trial structures at successive AM1, B3LYP/6-31G(d), and B3LYP/6-31++G(d,p) levels of theory[68] and reported 23 conformers

DOI: 10.1021/acs.jpcb.9b08796
J. Phys. Chem. B 2019, 123, 10410−10423

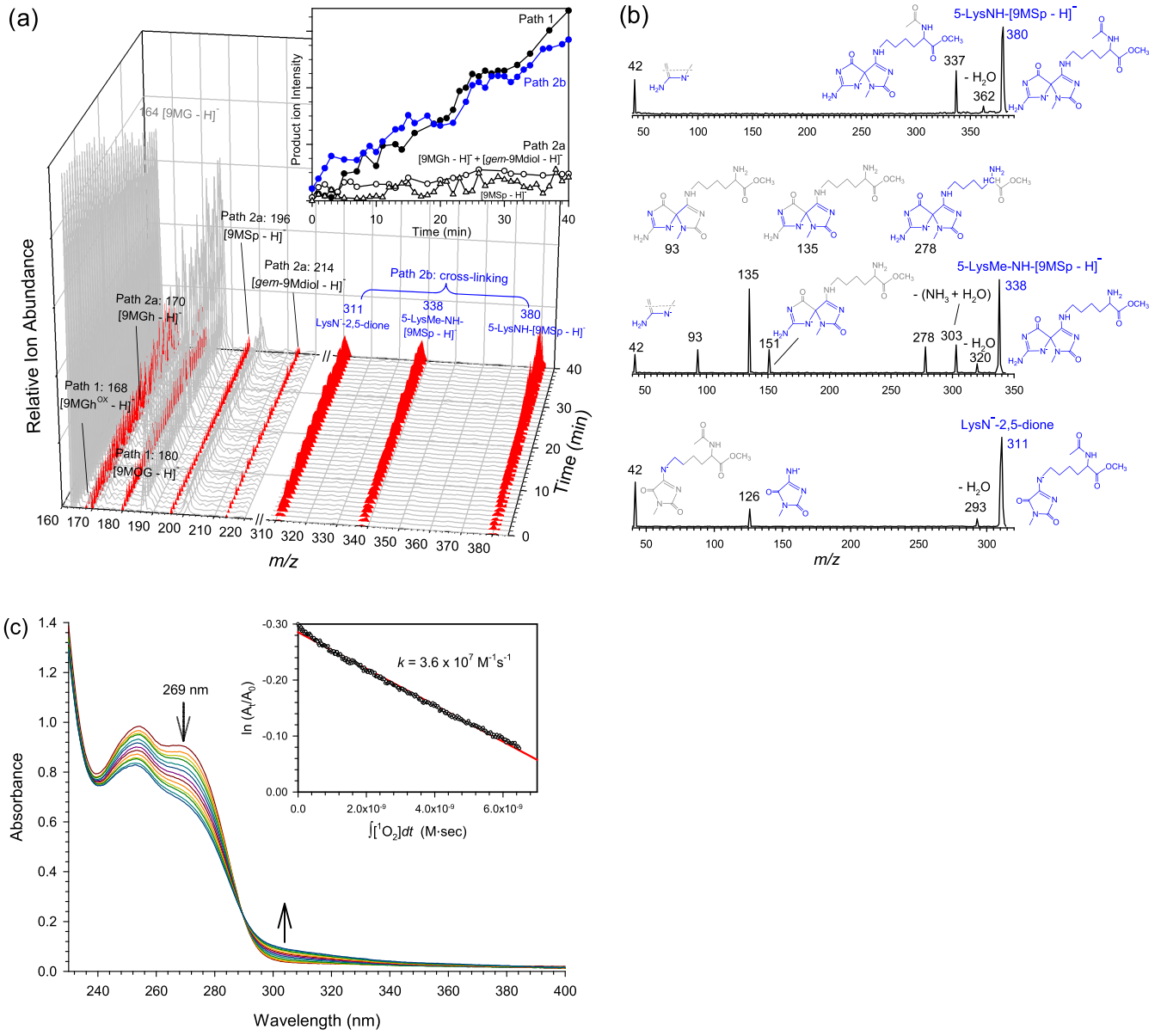

Figure 1. (a) Negative ESI MS for the reaction of $[9MG - H]^-$ + $LysNH_2$ + $^1O_2$ measured at pH 10.0, where all of the $^1O_2$-specific products are highlighted in red, and all gray peaks (except for the reactant ions as indicated) may be attributed to the background in solution or non-$^1O_2$-specific reactions. The inset shows relative product ion yields along the reaction time; (b) CID MS/MS of the cross-linking products, where blue structures represent the fragment ions observed and gray structures represent the portions of the molecule lost on CID; and (c) UV−vis absorption spectra and the plot of $\ln(A_t/A_0)$ vs $\int[^1O_2]_t\,dt$, where A_t and A_0 are the absorbance of $[9MG - H]^-$ at 269 nm at different times and time zero.

within an energy range of 10 kJ/mol at B3LYP/6-31++G(d,p). The set of low-energy structures was expanded by Boeckx et al.[69] These stable canonical lysine conformations were used as starting structures for building the input geometries of $LysNH_2$ (i.e., N^α-acetyl-lysine-methyl ester), and the torsion angles of the N^α-acetyl and the methyl ester groups were each rotated at 60° increments to create various trial rotamers. Every generated conformation was optimized using SMD-ωB97XD/6-31+G(d,p). It is to be noted that many intramolecular H-bonds of lysine were lost upon the substitutions of the $-COOH$ and $-N^\alpha H_2$ groups. Our calculations identified a total of 37 low-energy conformers for $LysNH_2$. Their structures, relative enthalpies, and Cartesian coordinates are provided in Figure S3 and in the Supporting Information.

On the basis of its pK_a values, $LysNH_2$ is completely protonated at pH 7.0 and consists of 78% protonated $LysNH_3^+$ and 22% neutral $LysNH_2$ at pH 10.0. $LysNH_2$ has three basic sites, which can be protonated: the $-N^\varepsilon H_2$ group (pK_a = 10.54[70]), the $-N^\alpha H$ group (pK_a = 1.25 estimated from that of protonated *N*-methylacetamide[71]), and the carbonyl oxygen of the *N*-acetyl group (as the charge in the ensuing $HNC{=}OH^+$ is stabilized by amide resonance with a protonated imine structure $HN^+{=}C\text{-}OH$).[72,73] To identify the global minimum $LysNH_3^+$, we calculated all three protonated structures for each of the first 10 low-energy $LysNH_2$ conformers in Figure S3. The resulting 32 protonated structures, their relative enthalpies at 298 K, and Cartesian coordinates are provided in Figure S4 and in the Supporting Information. The dominant protonated conformations belong to the structures of $-N^\varepsilon H_3^+$, of which the $LysNH_3^+$_1 conformer formed by protonation of the second lowest-energy $LysNH_2$ conformer accounts for a dominating protonated structure (45%).

DOI: 10.1021/acs.jpcb.9b08796
J. Phys. Chem. B 2019, 123, 10410−10423

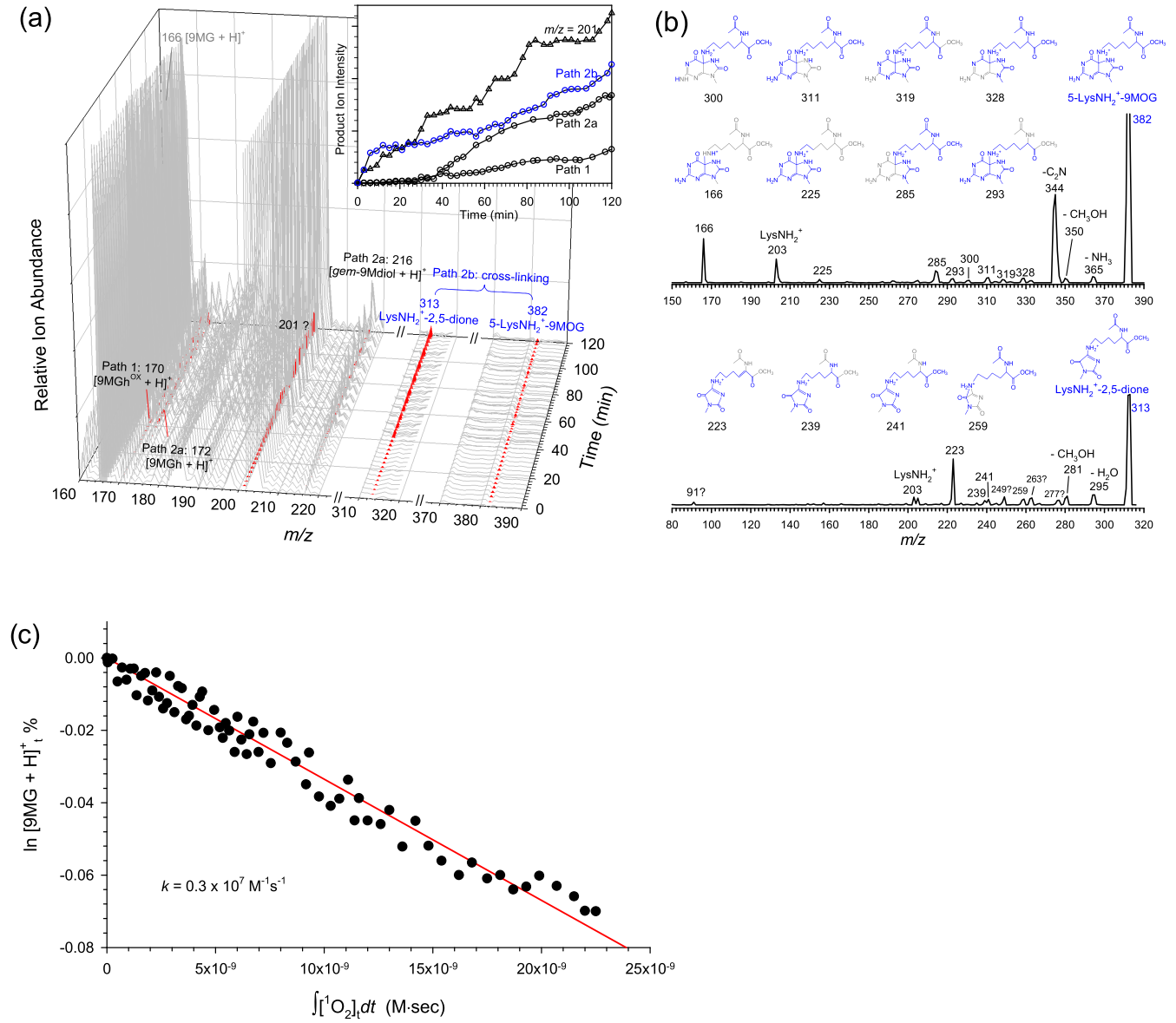

Figure 2. (a) Positive ESI MS for the reaction of 9MG + $LysNH_3^+$ + $^1O_2$ measured at pH 7.0, where all of the $^1O_2$-specific product ions are highlighted in red, and all gray peaks (except for the reactant ions as indicated) may be attributed to the background in solution or non-$^1O_2$-specific reactions. The inset shows relative product ion yields along the reaction time; (b) CID MS/MS of the cross-linking products, where blue structures represent the fragment ions observed and gray structures represent the portions of the molecule lost on CID; and (c) the plot of $\ln[9MG + H]^-_t$% vs $\int[^1O_2]_t\,dt$, where $[9MG + H]^-_t$% is the relative abundance of the reactant ion in the MS.

Due to the mixed open- and closed-shell characters of $^1O_2$,[9,74] closed-shell calculations failed to produce an accurate $^1O_2$ excitation energy; open-shell, broken-symmetry calculations, on the other hand, brought about significant spin contamination from $^3O_2$. Fortunately, the late-stage reaction intermediates and TSs (after the formation of endoperoxide) are all closed-shell and dominated by single electronic states[7] (as determined on the basis of T1 diagnostics);[75] thus, spin contamination would not influence these species significantly. To correct for spin contamination existing at the early stage of the reaction PES, electronic energy for open-shell singlet state was calculated using Yamaguchi's approximate spin-projection method[76,77]

$$E^{AP} = \frac{E^{BS}\langle \mathbf{S^2}\rangle^{HS} - E^{HS}\langle \mathbf{S^2}\rangle^{BS}}{\langle \mathbf{S^2}\rangle^{HS} - \langle \mathbf{S^2}\rangle^{BS}} \quad (1)$$

where E represents the electronic energy, with the superscript AP referring to the approximately spin-projected singlet state, BS the open-shell, broken-symmetry singlet state, and HS the triplet state, and $\langle \mathbf{S^2}\rangle$ represents spin contamination. The spin-projected $^1O_2$ excitation energy was calculated to be 96.5 kJ/mol at SMD-ωB97XD/aug-cc-pVQZ (the split-valence quadruple-zeta correlation-consistent basis set of Dunning and coworkers with added diffuse functions[78])//SMD-ωB97XD/6-31+G(d,p), consistent with the experimental value of 94.6 kJ/mol. It was also reported by Schlegel et al. that the ωB97XD level of theory produced reasonably good spin-projection results for the $^1O_2$ reaction with guanine.[26]

All of the PES calculations were carried out at a static level, which may lead to the overestimation of reaction barriers; fortunately, in the present $^1O_2$-induced reactions, the overall reaction profiles are all strongly exergonic. Note that ab initio

DOI: 10.1021/acs.jpcb.9b08796
J. Phys. Chem. B 2019, 123, 10410−10423

molecular dynamics simulations may help provide an even more robust description of reactions in the gas phase and with solvation, e.g., our dynamics simulations of the $^1O_2$ oxidation of guanine,[6] 9MG,[7] and guanine−cytosine base pair in the gas phase,[17] and Dumont et al.'s molecular dynamics work on the $^1O_2$ oxidation of guanine bases within B-DNA helix[27,28] and the cross-linking of polyamine[43] and trilysine peptide[44] with oligonucleotides.

4. RESULTS AND DISCUSSION

4.1. Product Distributions of 9MG Oxidation and 9MOG^{OX}−LysNH$_2$ Cross-Links. In our previous work,[9] the $^1O_2$ oxidation of 9MG was measured at pH 4.0, 7.0, and 10.0. After taking into account the populations of different ionization states of 9MG at each pH, the oxidation rate constant was determined to be 1.2×10^6 $M^{-1}\cdot s^{-1}$ for neural 9MG and $(4.6–4.9) \times 10^7$ $M^{-1}\cdot s^{-1}$ for deprotonated $[9MG - H]^-$. No oxidation was observed for protonated $[9MG + H]^+$. This pH dependence led us to focus on measuring $^1O_2$-oxidation-induced 9MOG^{OX}−LysNH$_2$ cross-links only at pH 7.0 and 10.0.

4.1.1. Products at pH 10.0. The oxidation of 9MG and the subsequent cross-linking with LysNH$_2$ were revealed by real-time MS and UV−vis absorption as shown in Figure 1. Psciuk and Schlegel have calculated the pK_a values for 9MG oxidation intermediates and products (including 9MOG, 9MOG^{OX}, 5-OH9MOG, *gem*-9Mdiol, 4-carboxy9MGh, 9MSp, and 9MGh), using solute cavity scaling to overcome the inaccuracies of standard implicit solvent methods.[24] Their results suggest that all intermediates and products are deprotonated at pH 10.0 and thus could be detected by negative ESI MS efficiently. According to the pK_a values of LysNH$_2$ (pK_a = 10.54[70]), 9MG (pK_{a2} = 9.56),[50] and 9MG oxidation products, it is reasonable to assume that at pH 10.0 the LysNH moiety of the cross-links remained in the neutral state, whereas the 9MG moiety was deprotonated. All of the $^1O_2$-specific product ions are highlighted in red in the mass spectra of Figure 1a. Except for the reactant ions of *m*/*z* 164, all of the ion peaks in gray represent background species in the solution or the non-$^1O_2$-specific products. $^1O_2$-specific products include $[9MGh^{OX} - H]^-$ (*m*/*z* 168) and $[9MOG - H]^-$ (*m*/*z* 180), which were produced via Path 1 (see Scheme 1), $[9MGh - H]^-$ (*m*/*z* 170), $[9MSp - H]^-$ (*m*/*z* 196), and $[gem\text{-}9Mdiol - H]^-$ (*m*/*z* 214) via Path 2a, and 5-LysNH−$[9MSp - H]^-$ (*m*/*z* 380) via Path 2b. Secondary products arising from cross-links were detected, too, including 5-LysMe−NH−$[9MSp - H]^-$ (*m*/*z* 338, produced via the N^{α}-acetyl hydrolysis of 5-LysNH−$[9MSp - H]^-$) and 1-methyl-4-LysN$^-$−2,5-dihydro-1*H*-imidazoline-2,5-dione (*m*/*z* 311, abbreviated as LysN$^-$−2,5-dione, produced by CO elimination and subsequent hydrolysis of 5-LysNH−$[9MSp - H]^-$, vide infra). None of these products were observed in the control experiment using $^3O_2$.

The inset of Figure 1a shows the appearance and the relative abundances of all product ions throughout the 40 min reaction, where the products produced from the same reaction pathway were combined. The final product branching ratios are Path 1 (9MGh^{OX} + 9MOG) = 0.47: Path 2a (9MGh + 9MSp + *gem*-9Mdiol) = 0.13: Path 2b (cross-linking) = 0.40. For comparison, product branching ratios measured at the same pH but in the absence of LysNH$_2$ were Path 1 = 0.28: Path 2a = 0.72. This is consistent with the previous finding that 9MG−LysNH$_2$ cross-links compete with 9MSp.[34] We have also examined the reaction at pH 10.0 using low concentrations of LysNH$_2$ (0.5−1.0 mM), in which case 9MG^{OX}−LysNH$_2$ cross-links were not observed at all.

All of the product ions were subjected to CID with Xe gas for structural characterization. The CID product ion mass spectra of $[9MGh^{OX} - H]^-$, $[9MGh - H]^-$, $[9MOG - H]^-$, $[9MSp - H]^-$, and $[gem\text{-}9Mdiol - H]^-$ are identical to those reported before[9] and thus not shown here. Figure 1 depicts the CID results of the cross-links. As shown by the ChemDraw structures in Figure 1b, the fragment ions of 5-LysNH−$[9MSp - H]^-$, 5-LysMe−NH−$[9MSp - H]^-$, and LysN$^-$−2,5-dione could be rationalized by their partial structures where blue-colored structures represent the fragment ions observed in the CID mass spectra and gray-colored structures depict the portions of the molecule lost upon CID.

Dramatic bleaching of 9MG absorbance was observed throughout the reaction. As illustrated in Figure 1c, the decrease of 9MG absorbance in the range of 240−290 nm was accompanied by the increasing product absorption above 290 nm, with an isosbestic point located at 290 nm.

4.1.2. Products at pH 7.0. The oxidation and cross-linking of 9MG became much slower under the neutral condition. The change of the UV−vis absorbance of the reaction solution was less than 1% over a 1 h reaction period. The $^1O_2$-specific oxidation products detected in the positive ESI MS (Figure 2a) include $[9MGh^{OX} + H]^+$ (*m*/*z* 170, Path 1), $[9MGh + H]^+$ and $[gem\text{-}9Mdiol + H]^+$ (*m*/*z* 172 and 216, Path 2a), and product ions at *m*/*z* 201. However, no $[9MSp + H]^+$ was observed in the presence of LysNH$_2$. On the other hand, the product ions of *m*/*z* 201 were observed in both the absence[9] and the presence of LysNH$_2$. As reported in our previous study,[9] *m*/*z* 201 resembled 5-carboxamido-5-formamido-2-iminohydantoin (2Ih),[79] in that they have shown the same CID fragmentation pattern, albeit that protonated 9-methyl-2Ih corresponds to *m*/*z* 200.

The cross-links detected at pH 7.0 include 5-LysNH$_2^+$−9MOG (*m*/*z* 382) and 1-methyl-4-LysNH$_2^+$−2,5-dihydro-1*H*-imidazoline-2,5-dione (*m*/*z* 313, abbreviated as LysNH$_2^+$−2,5-dione). The latter was produced by the CO elimination of 5-LysNH$_2^+$−9MOG (vide infra) followed by the hydrolysis of the ensuing guanidine intermediate. Note that at pH 7.0, the LysNH moiety is completely protonated. This implies that all stable cross-linking products could be detected by positive ESI MS. We also note that *m*/*z* 382 could be possibly assigned to 5-LysNH$_2^+$−9MSp, a protonated analogue of 5-LysNH−$[9MSp - H]^-$ that was detected at pH 10.0. However, the reaction PES analysis (to be discussed below) has suggested that the formation of 5-LysNH$_2^+$−9MSp was not possible.

The inset of Figure 2a presents the products growing and their relative abundances as a function of reaction time, for a total reaction duration of 2 h. The final product branching ratios are Path 1 (9MGh^{OX}) = 0.08: Path 2a (9MGh + *gem*-9Mdiol) = 0.22: Path 2b (cross-linking) = 0.29: *m*/*z* 201= 0.41. The product branching ratios changed to Path 1 (9MGh^{OX}) = 0.20: Path 2a (9MSp + 9MGh) = 0.32 + 0.25 = 0.57: *m*/*z* 201= 0.23 in the absence of LysNH$_2$. Again, the cross-links became insignificant when the LysNH$_2$ concentration was lowered to 1.0 mM.

The structures of all protonated product ions were also examined by CID MS/MS. The CID results of $[9MGh^{OX} + H]^+$, $[9MGh + H]^+$, $[gem\text{-}9Mdiol + H]^+$, and *m*/*z* 201 were reported before.[9] Figure 2b depicts the CID results of 5-LysNH$_2^+$−9MOG and LysNH$_2^+$−2,5-dione. Most of the

DOI: 10.1021/acs.jpcb.9b08796
J. Phys. Chem. B 2019, 123, 10410−10423

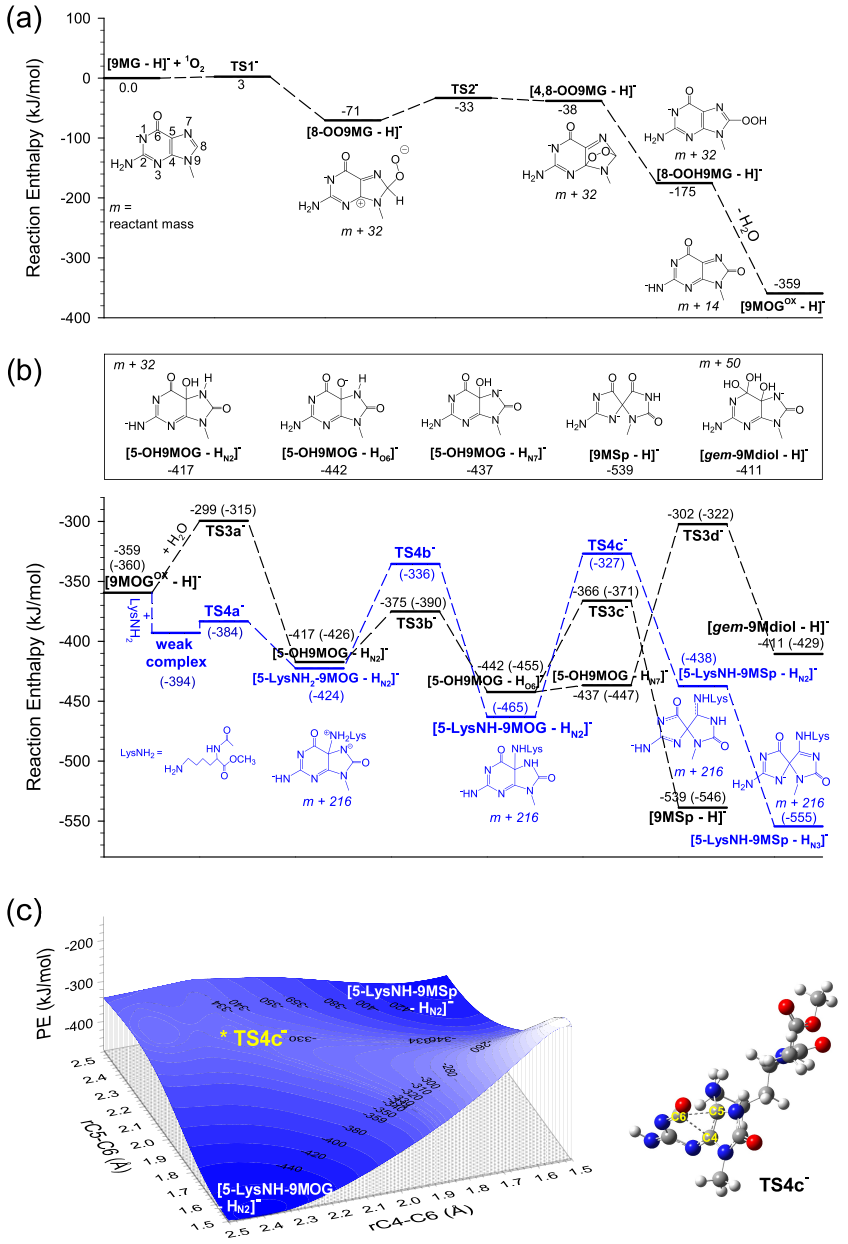

Figure 3. (a, b) Reaction PES for the $^1O_2$ oxidation of $[9MG - H]^-$ and the cross-linking of $[9MOG^{OX} - H]^-$ with $LyNH_2$. All structures and energies were calculated at SMD-ωB97XD/aug-cc-pVQZ//SMD-ωB97XD/6-31+G(d,p), except for those listed in parentheses, which were calculated at SMD-ωB97XD/6-31+G(d,p). Reaction enthalpies included ZPEs and thermal corrections at 298 K. Structures of TSs are available in the Supporting Information; and (c) relaxed 2D-PES for the conversion of $[5\text{-LysNH}{-}9MOG - H_{N2}]^-$ to $[5\text{-LysNH}{-}9MSp - H_{N2}]^-$ via TS4c$^-$. Numbers in the contour map are reaction energies (without ZPE and thermal corrections) calculated at SMD-ωB97XD/6-31+G(d,p).

fragment ions of 5-$LysNH_2^+$−9MOG and $LysNH_2^+$−2,5-dione could be explained by their partial structures. Note that one major fragment ion m/z 344 of 5-$LysNH_2^+$−9MOG corresponds to the elimination of C_2N; however, its dissociation mechanism remains unclear. It is likely that C_2N elimination involves the decomposition and rearrangement of aromatic rings.

Since the reaction at pH 7.0 resulted in only subtle changes in the UV−vis spectroscopy, the oxidation kinetics of 9MG was determined by measuring the abundance of the remaining 9MG in the product mass spectra. The kinetics data is plotted in Figure 2c.

4.2. Reaction PESs. Schlegel and co-workers[26] calculated the $^1O_2$ oxidation of guanine and the formation of guanine−lysine cross-links at the SMD-ωB97XD/aug-cc-pVTZ//SMD-ωB97XD/6-31+G(d,p) levels of theory, in which the lysine molecule was modeled using $MeNH_2$. In our previous study of the $^1O_2$ oxidation of guanine and 9MG,[9] we had used their study as a guide to refine reaction surfaces using a large basis set SMD-ωB97XD/aug-cc-pVQZ//SMD-ωB97XD/6-31+G-(d,p) and expanded the reaction systems to include neutral, protonated, and deprotonated guanine and 9MG. In the present work, we have continued using Schlegel et al.'s work[26] as a guide and expanded calculations to include the cross-linking of $9MGh^{OX}$ with the full molecular structure of $LysNH_2$. The calculations were focused on two specific reaction systems: one is the $^1O_2$ oxidation of $[9MG - H]^-$ and the cross-linking of the ensuing $[9MOG^{OX} - H]^-$ with

DOI: 10.1021/acs.jpcb.9b08796
J. Phys. Chem. B 2019, 123, 10410−10423

neutral $LysNH_2$, which represents the experiment at pH 10.0, and the other is the oxidation of neutral 9MG followed by cross-linking with protonated $LysNH_3^+$, which is to mimic the reaction at pH 7.0.

4.2.1. PES for pH 10.0. Figure 3 reports the PES for $[9MG - H]^- + {}^1O_2 + LysNH_2$ that is the computational equivalent of a reaction at pH 10.0, where $LysNH_2$ was predominantly neutral, whereas the 9MG reactant and its oxidation intermediates were deprotonated judged by their experimental[50] or calculated[24] pK_a values. The global minimum conformer of each reactant was used as the starting structure in the reaction coordinate calculation. Cartesian coordinates of all calculated species are provided in the Supporting Information, including GaussView structures of TSs. Figure 3a summarizes the oxidation process of $[9MG - H]^-$. The reaction starts with an addition of ${}^1O_2$ to the C8 of $[9MG - H]^-$ to form an 8-peroxide $[8\text{-}OO9MG - H]^-$ via $TS1^-$. Of the different ionization states of 9MG, $[9MG - H]^-$ bears the lowest activation barrier (3 kJ/mol) for the initial O_2 attack (for comparison, the barrier raises to 25 kJ/mol for neutral 9MG and 50 kJ/mol for protonated $[9MG + H]^+$).[9] This is consistent with the experiment where the reaction was the fastest in a basic solution. $[8\text{-}OO9MG - H]^-$ evolves to a 4,8-endoperoxide $[4,8\text{-}OO9MG - H]^-$ via $TS2^-$.[7,9] The latter subsequently transforms into $[8\text{-}OOH9MG - H]^-$ via an H-atom transfer from the C8 atom to the C8-OO terminal, followed by the elimination of water to form $[9MOG^{OX} - H]^-$. No significant barriers would be expected for these transformations.[9,26]

Figure 3b depicts the nucleophilic reactions of $[9MOG^{OX} - H]^-$ with water and $LyNH_2$. The two reactions can be distinguished by different colors, and their main points are described here:

(1) C5-water addition: Water addition to $[9MOG^{OX} - H]^-$ needs to cross an energy barrier at $TS3a^-$. In the presence of two water molecules (one water acts as a reactant and the other is catalytic),[26] the activation energy of $TS3a^-$ is reduced to 60 kJ/mol with respect to the intermediate $[9MOG^{OX} - H]^- + H_2O$ prior to the transition state (or 299 kJ /mol below the starting reactants). The initial adduct $[5\text{-}OH9MOG - H_{N2}]^-$ (i.e., deprotonated at N2) undergoes water-assisted proton rearrangement (i.e., $TS3b^-$) and isomerizes to $[5\text{-}OH9MOG - H_{O6}]^-$ (i.e., deprotonated at O6) and then to $[5\text{-}OH9MOG - H_{N7}]^-$ (i.e., deprotonated at N7). $[5\text{-}OH9MOG - H_{O6}]^-$ may convert to $[9MSp - H]^-$ via an acyl shift at $TS3c^-$ (barrier height is 76 kJ/mol above $[5\text{-}OH9MOG - H_{O6}]^-$ but 366 kJ/mol below the starting $[9MG - H]^-$), and $[5\text{-}OH9MOG - H_{N7}]^-$ may convert to $[gem\text{-}9Mdiol - H]^-$ via $TS3d^-$ (135 kJ/mol above $[5\text{-}OH9MOG - H_{N7}]^-$ but 302 kJ/mol below the starting reactants) with the aid of two water molecules; see the structure in the Supporting Information. $TS3c^-$ is located 64 kJ/mol lower in energy than $TS3d^-$, but the product yield of $[gem\text{-}9Mdiol - H]^-$ (including its derivate $[9MGh - H]^-$) is compatible with that of $[9MSp - H]^-$ as shown in the inset of Figure 1a. On the other hand, $[9MSp - H]^-$ was indeed more favorable than $[gem\text{-}9Mdiol - H]^-$ and $[9MGh - H]^-$ in the absence of $LysNH_2$. This implies that the yields of $[9MSp - H]^-$, $[gem\text{-}9Mdiol - H]^-$, and $[9MGh - H]^-$ were affected differently by the presence of $LysNH_2$.

(2) C5-$LysNH_2$ addition: We have tried to map out the whole PES at the SMD-ωB97XD/aug-cc-pVQZ//SMD-ωB97XD/6-31+G(d) levels of theory, but single-point calculations of the cross-linking structures were not able to converge using the aug-cc-pVQZ basis set. Therefore, the PES energetics for the portion of $9MOG^{OX}$–$LysNH_2$ cross-linking were calculated at SMD-ωB97XD/6-31+G(d). We have compared reaction energetics for C5-water addition at SMD-ωB97XD/aug-cc-pVQZ//SMD-ωB97XD/6-31+G(d) vs SMD-ωB97XD/6-31+G(d). The results are listed in Figure 3b. Energy differences between the two sets of calculations are no more than 20 kJ/mol. Considering the relatively small variations, it is feasible to compare the C5-water and C5-$LysNH_2$ addition PESs at either level of theory.

On the basis of a relaxed PES scan along the approaching distance between the C5 of $[9MOG^{OX} - H]^-$ and the N^{ϵ} of $LysNH_2$, $[9MOG^{OX} - H]^-$ and $LysNH_2$ first form an electrostatic complex with a binding energy of 34 kJ/mol. This complex serves as a precursor for the formation of a covalent complex $[5\text{-}LysNH_2\text{–}9MOG - H_{N2}]^-$ via $TS4a^-$. $TS4a^-$ is located 10 kJ/mol above the precursor complex but 24 kJ/mol below the sum of $[9MOG^{OX} - H]^- + LysNH_2$ (and 394 kJ/mol below the starting reactants). In other words, the C5-addition of $LysNH_2$ is barrierless. $[5\text{-}LysNH_2\text{–}9MOG - H_{N2}]^-$ isomerizes to $[5\text{-}LysNH\text{–}9MOG - H_{N2}]^-$ via a proton transfer from the lysine $N^{\epsilon}H_2$ to the N7 of 9MOG at $TS4b^-$. The latter complex undergoes a 1,2-shift of the acyl group via $TS4c^-$ and results in the formation of a spiro product $[5\text{-}LysNH\text{–}9MSp - H_{N2}]^-$ and its more stable isomer $[5\text{-}LysNH\text{–}9MSp - H_{N3}]^-$.

To examine the reaction surface for the acryl shift in detail and determine if there exist other stable products, a 21 × 20 grid 2D-PES was generated at the SMD-ωB97XD/6-31+G(d) level of theory. In the relaxed 2D-PES scan, the two bond lengths rC5–C6 (the breaking bond in $[5\text{-}LysNH\text{–}9MOG - H_{N2}]^-$) and rC4–C6 (the new bond formed in $[5\text{-}LysNH\text{–}9MSp - H_{N2}]^-$) varied from 1.5 to 2.55 Å and from 2.5 to 1.5 Å, respectively, at an interval of 0.05 Å. All of the other bond lengths and bond angles were optimized at each point of the PES. The contour map is visualized in Figure 3c, in which the changes in electronic energy are depicted. On this PES, there are two deep potential wells corresponding to $[5\text{-}LysNH\text{–}9MOG - H_{N2}]^-$ and $[5\text{-}LysNH\text{–}9MSp - H_{N2}]^-$, respectively, and a saddle point (i.e., $TS4c^-$) located at rC5–C6 = 2.15 Å and rC4–C6 = 2.25 Å, which leads an intrinsic reaction coordinate from the reactant to the spiro product with an activation energy of 137 kJ/mol above $[5\text{-}LysNH\text{–}9MOG - H_{N2}]^-$.

Our PES results are in good agreement with the previous study of Schlegel et al.[26] According to the PES analysis, C5-water addition is rate-limited by $TS3a^-$ (60 kJ/mol above the sum of $[9MOG^{OX} - H]^- + H_2O$, 299 kJ/mol below the starting $[9MG - H]^- + {}^1O_2$), whereas C5-$LysNH_2$ addition is barrierless with respect to $[9MOGOX - H]^- + LysNH_2$. Downhill, $TS4b^-$ and $TS4c^-$ that lead to spiro $[5\text{-}LysNH\text{–}9MSp - H_{N2}]^-$ are both lower in energy than $TS3a^-$. The formation of $[gem\text{-}9Mdiol - H]^-$ is controlled by another rate-

DOI: 10.1021/acs.jpcb.9b08796
J. Phys. Chem. B 2019, 123, 10410–10423

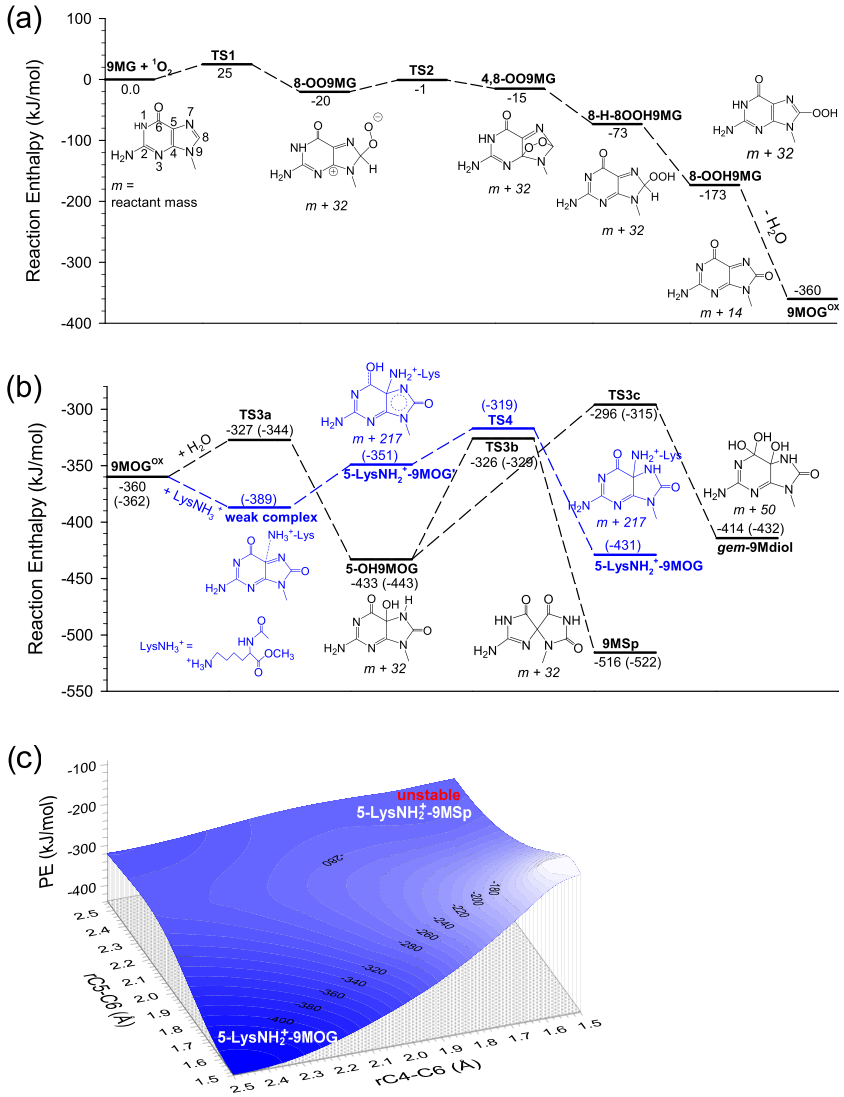

Figure 4. (a, b) Reaction PES for the oxidation of 9MG by $^1O_2$ and the cross-linking of 9MOG^{OX} with $LyNH_3^+$. All structures and energies were calculated at SMD-ωB97XD/aug-cc-pVQZ//SMD-ωB97XD/6-31+G(d,p), except for those listed in parentheses, which were calculated at SMD-ωB97XD/6-31+G(d,p). Reaction enthalpies included ZPEs and thermal corrections at 298 K. Structures of TSs are available in the Supporting Information; and (c) relaxed 2D-PES exploring the structures of 5-LysNH$_2^+$−9MOG and 5-LysNH$_2^+$−9MSp. It shows that 5-LysNH$_2^+$−9MSp is not a stationary structure on the reaction surface. Numbers in the contour map are reaction electronic energies (without ZPE and thermal corrections) calculated at SMD-ωB97XD/6-31+G(d,p).

limiting barrier TS3d$^-$ whose activation energy is comparable to TS3a$^-$. The comparison of barrier heights for the formation of [9MSp − H]$^-$, [*gem*-9Mdiol − H]$^-$, and [5-LysNH−9MSp − H_{N2}]$^-$ has provided a qualitative explanation for the fact that at pH 10.0 the product branching ratio for $LysNH_2$ cross-links is nearly a factor of 3 higher than that of [9MSp − H]$^-$ + [*gem*-9Mdiol − H]$^-$.

4.2.2. PES for pH 7.0. The PES for 9MG + $^1O_2$ + $LysNH_3^+$ is summarized in Figure 4. Here, only the differences compared to the pathways at pH 10 and the kinetics consequences are addressed:

(1) Similar to that of [9MG − H]$^-$, the stepwise $^1O_2$ addition to neutral 9MG first results in the formation of 8-OO9MG (Figure 4a). However, the rate-limiting barrier TS1 is 22 kJ/mol higher than its deprotonated analogue TS1$^-$; as a result, 9MG becomes much less reactive toward $^1O_2$. Besides, the conversion of the endoperoxide 4,8-OO9MG to hydroperoxide 8-OOH9MG may be mediated by N1-deprotonation and protonation of an 8-H-8-OOH9MG intermediate, the latter may not form for [9MG − H]$^-$.

(2) For C5-water addition, the barriers of TS3a leading to 5-OH9MOG, TS3b leading to 9MSp and TS3c to *gem*-9Mdiol are 33, 34 and 64 kJ/mol, respectively, relative to 9MOG^{OX} + H_2O (or 327, 326, and 296 kJ/mol, respectively, below the starting reactants). For comparison, their deprotonated counterparts TS3a$^-$, TS3b$^-$ and TS3c$^-$ are 60, −16 and −7 kJ/mol with respect to [9MOG^{OX} − H]$^-$ + H_2O (or −299, −375, and −366 kJ/mol with respect to the starting reactants). The changes of C5-water reaction barriers for neutral vs deprotonated 9MOG^{OX} indicate that the formation of neutral 9MSp becomes less favorable. Note that, without the participation of $LysNH_3^+$, we were able to detect a low yield of 9MSp at pH 7.0.[9,13] The shutdown of the 9MSp channel in the presence of $LysNH_3^+$ (see Figure

DOI: 10.1021/acs.jpcb.9b08796
J. Phys. Chem. B 2019, 123, 10410−10423

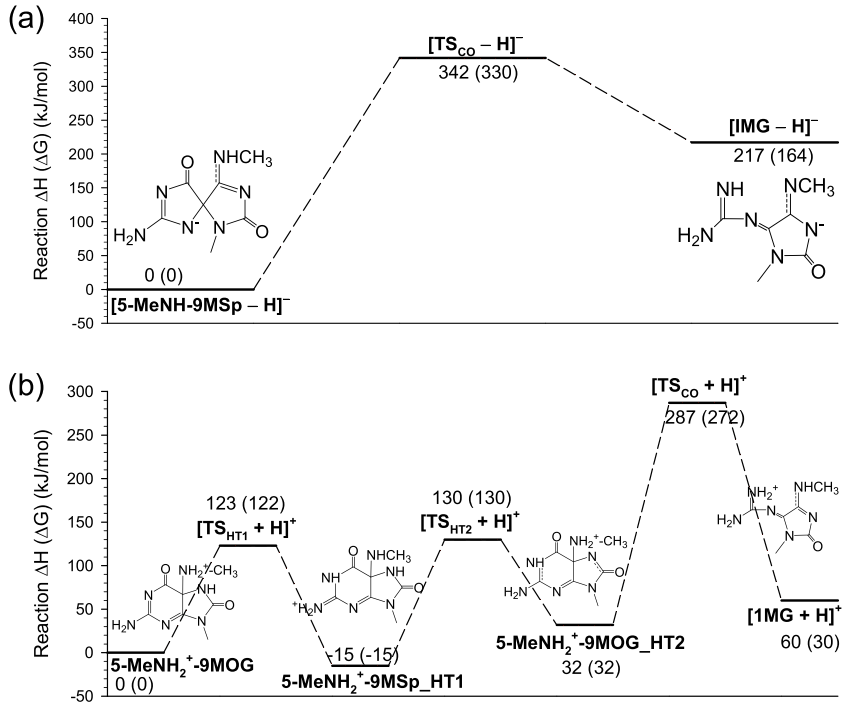

Figure 5. SMD-ωB97XD/6-31+G(d)-calculated PESs for CO elimination of (a) [5-MeNH−9MSp − H]$^-$ and (b) 5-MeNH$_2^+$−9MOG. Energies indicated are reaction enthalpies and changes of free energy (in parentheses). Structures of TSs are available in the Supporting Information.

2a) verifies the additional suppression of 9MSp by LysNH$_3^+$. On the other hand, both [9MGh + H]$^+$ and [*gem*-9Mdiol + H]$^+$ were observed in the presence of LysNH$_3^+$.

(3) The last yet the most significant difference concerns the cross-linking of 9MOG^{OX} with LysNH$_2$. The cross-linking of 9MOG^{OX} and LysNH$_3^+$ produces only 5-LysNH$_2^+$−9MOG′ (and its more stable isomer 5-LysNH$_2^+$−9MOG). We attempted to locate a stable spiro product by running a relaxed 2D-PES scan along the acyl shift reaction coordinates, i.e., rC4−C6 and rC5−C6 of 5-LysNH$_2^+$−9MOG, and the result is depicted in Figure 4c. In contrast to the 2D-PES of Figure 3c for the acyl shift of [5-LysNH−9MOG − H$_{N2}$]$^-$ → [5-LysNH−9MSp − H$_{N2}$]$^-$, 5-LysNH$_2^+$−9MOG represents the only minimum on the PES of Figure 4c. 5-LysNH$_2^+$−9MSp is completely unstable, located at a strip of high-lying (>150 kJ/mol above LysNH$_2^+$−9MOG) and descending surface. There is no obvious saddle point, which leads to the formation of 5-LysNH$_2^+$−9MSp from 5-LysNH$_2^+$−9MOG. The studies of Schlegel et al. on guanine−lysine adduct formation also found that acyl migration requires anionic states (and in a few cases, neutrals).[26,42]

The reaction barrier TS4 for 9MOG^{OX} + LysNH$_3^+$ is comparable to TS3a and TS3b but lower than TS3c; the latter is the barrier leading to the formation of *gem*-9Mdiol. These calculation results are consistent with the experimental finding that the product branching ratio for cross-links (path 2b) is slightly higher than that for path 2a (*gem*-9Mdiol + 9MGh, see Figure 2a).

4.2.3. Formation of LysNH−2,5-dione by In-Source Collisions. The LysNH−2,5-dione products identified in our MS and MS/MS analyses were not observed in Burrows et al.'s experiments.[34,41] We have explored their formation pathways at the SMD/ωB97XD/6-31+G(d) level. To lower the computational cost, LysNH$_2$ was modeled by methylamine. The formation pathway for the 2,5-dione is pH-dependent. Deprotonated LysN$^-$−2,5-dione (m/z 311) was likely formed via CO elimination of [5-LysNH−9MSp − H]$^-$, as illustrated in Figure 5a where CH$_3$NH$_2$ was used to mimic LysNH$_2$. The ensuing *N*-[2,3-dihydro-3-methyl-5-(methylamino)-2-oxo-4*H*-imidazol-4-ylidene]-guanidine (in its deprotonated form, abbreviated as [IMG − H]$^-$) was susceptible to hydrolysis and lost the guanidine group upon reacting with water (similar to the loss of a guanidine group via hydrolysis of nucleoside[36,80]). Reaction pathway changes when 5-LysNH$_2^+$−9MOG dominated the cross-links at pH 7. As shown in Figure 5b, CO elimination is now initiated by two successive intramolecular H transfer of 5-RNH$_2^+$−9MOG, leading to the formation of 5-RNH$_2^+$−9MOG_HT2. The latter eliminates CO via [TS$_{CO}$ + H]$^+$, and the resulting [IMG + H]$^+$ is hydrolyzed to RNH$_2^+$−2,5-dione (i.e., m/z 313 in Figure 2a).

The PESs in Figure 5 involve transition states between various intermediates. Despite the fact that none of these activation barriers are located above the starting reactants of 9MG + ^{1}O$_2$ + RNH$_2$, these barriers might be too high for the reactions to occur in solution.[34,41] We tend to attribute the formation of the 2,5-dione products to the in-source collisions and reactions with water during the online MS, where the sample solution was transported to the mass spectrometer through a heated desolvation capillary and then accelerated in an electrical field between the exit of the capillary and a skimmer. Consequently, product ions underwent thermal decomposition and collision-induced dissociation with the background gas (including water vapor) in the source chamber. These could presumably facilitate crossing reaction barriers and forming the 2,5-dione products from [LysNH−9MSp − H]$^-$ and 5-LysNH$_2^+$−9MOG.

DOI: 10.1021/acs.jpcb.9b08796
J. Phys. Chem. B 2019, 123, 10410−10423

Table 1. Reaction Rate Constants and Product Branching Ratios

	rate constant ($M^{-1}\cdot s^{-1}$)		product branching ratio[a]	
pH	9MG + $^1O_2$	9MG + $^1O_2$ + $LysNH_2$	9MG + $^1O_2$	9MG + $^1O_2$ + $LysNH_2$
10.0	4.6×10^7	3.6×10^7	9MSp:(*gem*-9Mdiol + 9MGh):(9MOG + $9MGh^{OX}$) = 0.72:0.09:0.19	9MSp:(*gem*-9Mdiol + 9MGh):(9MOG + $9MGh^{OX}$):cross-links = 0.07:0.06:0.40:0.47
7.0	0.12×10^7	0.3×10^7	9MSp:(*gem*-9Mdiol + 9MGh):$9MGh^{OX}$ = 0.45:0.33:0.22	9MSp:(*gem*-9Mdiol + 9MGh):$9MGh^{OX}$:cross-links = 0:0.37:0.14:0.49

[a]Measured at the end of reactions. *m*/*z* 201 was not included in calculating the branching ratios at pH 7.0.

4.3. Reaction Kinetics. According to the calibration results of effective [$^1O_2$] in the reaction solutions (see details in the Supporting Information), 58% of solution-phase $^1O_2$ was physically quenched by collisions with 15 mM $LysNH_2$ (most likely due to its amide group[81]). Consequently, the $^1O_2$ oxidation of 9MG in the presence of $LysNH_2$ appeared to be much slower compared to that in the pure 9MG solution. In the following kinetics analysis, the physical quenching of $^1O_2$ by $LysNH_2$ was corrected for.

The reaction PESs suggest that the oxidation of 9MG and the subsequent cross-linking with $LysNH_2$ involve multiple steps. Among these steps, the initial addition of 9MG/$[9MG - H]^-$ + $^1O_2$ → TS1/$TS1^-$ → 8-OO9MG/$[8\text{-}OO9MG - H]^-$ is always the rate-limiting step and their reverse step may be discounted because the reverse reaction barriers are 20−71 kJ/mol higher than the forward ones. None of the subsequent reactions (including C5-water addition and C5-$LysNH_2$ cross-linking) encounter barriers above the starting reactants and therefore are expected to happen readily. It follows that the oxidation of 9MG in the presence of $LysNH_2$ may still be treated as first-order consecutive reactions, as it was in the absence of $LysNH_2$.[9] The overall kinetics for $[9MG - H]^-$ + $^1O_2$ + $LysNH_2$ may be described by eq 2 and its integrated form eq 3

$$-\frac{d[9MG - H]^-}{dt} = k[9MG - H]^-[^1O_2] \quad (2)$$

$$\ln[9MG - H]_t^-\% = \ln \frac{[9MG - H]_t^-}{[9MG - H]_t^- + [9MGh^{OX} - H]_t^- + [9MGh - H]_t^- + [9MOG - H]_t^- + [9MSp - H]_t^- + [gem - 9Mdiol - H]_t^- + [cross - links]_t} = -k\int [^1O_2]_t\, dt \quad (3)$$

where $[9MG - H]_t^-$, $[9MGh^{OX} - H]_t^-$, $[9MGh - H]_t^-$, $[9MOG - H]_t^-$, $[9MSp - H]_t^-$, $[gem\text{-}9Mdiol - H]_t^-$, and $[cross\text{-}links]_t$ represent the reactant and individual product concentrations, and $[9MG - H]_t^-\%$ is the remaining reactant abundance at reaction time *t*. In the experiment, $[9MG - H]_t^-\%$ was measured using UV−vis absorption spectra. As shown in Figure 1c, the plot of ln $[9MG - H]_t\%$ vs $\int [^1O_2]_t\, dt$ fits into a linear relationship, from which *k* was determined to be 3.6×10^7 $M^{-1}\cdot s^{-1}$. Rate constants for individual reaction pathways were estimated from the final product distributions, that is, 1.7×10^7 $M^{-1}\cdot s^{-1}$ for Path 1 (= $[9MGh^{OX} - H]^-$ + $[9MOG - H]^-$), 0.5×10^7 $M^{-1}\cdot s^{-1}$ for Path 2a (= $[9MGh - H]^-$ + $[9MSp - H]^-$ + $[gem\text{-}9Mdiol - H]^-$), and 1.4×10^7 $M^{-1}\cdot s^{-1}$ for Path 2b (cross-links).

The same first-order kinetics was used to analyze the reaction at pH 7.0. As mentioned above, the reaction rate decreased dramatically at pH 7.0, and no obvious bleaching of 9MG was observed during the reaction. We therefore chose to determine the rate constant on the basis of the abundances of the reactant and the product ions in the MS measurement. The decay of reaction ion abundance throughout the reaction is shown in Figure 2c, from which the reaction rate constant was determined to be 0.3×10^7 $M^{-1}\cdot s^{-1}$. The rate constants for individual product channels are 0.02×10^7 $M^{-1}\cdot s^{-1}$ for Path 1, 0.07×10^7 $M^{-1}\cdot s^{-1}$ for Path 2a, 0.09×10^7 $M^{-1}\cdot s^{-1}$ for Path 2b, and 0.12×10^7 $M^{-1}\cdot s^{-1}$ for *m*/*z* 201.

Table 1 summarizes the rate constants and product branching ratios for various systems and conditions. It is informative to investigate the influence of cross-linking on other product branchings. The most dramatic change is the product branching ratio of 9MSp, which is 0.72 in the absence of $LysNH_2$ vs 0.07 in the presence of $LysNH_2$ at pH 10.0 and changes to 0.45 vs 0.0 at pH 7.0. Such contrasting branching ratios reflect direct competition between the formation of 9MSp and 5-$LysNH_2$−9MSp. On the other hand, the formation of *gem*-9Mdiol and 9MGh was not affected at all. Their product branching ratio has remained at 0.06−0.09 at pH 10.0 and 0.33−0.37 at pH 7.0 (albeit that the formation of *gem*-9Mdiol and 9MGh needs the intermediacy of 5-OH9MOG and thus would have been expected to decrease in the presence of another nucleophile). The changes of 9MOG and $9MGh^{OX}$ yields in the presence of $LysNH_2$ appear to be irregular, increasing from 0.19 to 0.40 at pH 10.0 but decreasing from 0.22 to 0.14 at pH 7.0. Finally, *m*/*z* 201 maintains a relatively high yield in the pH 7.0 product, accounting for 25% of the total products in the reaction of 9MG and 40% in that of 9MG + $LysNH_2$.

5. CONCLUSIONS

The reaction of 9MG with $^1O_2$ and the cross-linking of the $9MOG^{OX}$ intermediate with $LysNH_2$ were investigated in the aqueous solution of pH 7.0 and 10.0. Online ESI MS and UV−vis absorption were utilized to measure reaction kinetics and product branching ratios. Product structures were characterized using CID MS/MS, and their reaction mechanisms were explored using a combination of SMD-ωB97XD/aug-cc-pVQZ and SMD-ωB97XD/6-31+G(d,p). Combined with our previous investigation of the pH-dependent $^1O_2$ oxidation of pure 9MG in aqueous solution,[9] we were able to track the changes of 9MG oxidation behaviors in the presence of two different

DOI: 10.1021/acs.jpcb.9b08796
J. Phys. Chem. B 2019, 123, 10410−10423

nucleophiles water and $LysNH_2$. It was found that, after correcting for the physical quenching of $^1O_2$ by $LysNH_2$, the overall rate constants in the presence and the absence of cross-linking are comparable and both have presented first-order kinetics in terms of 9MG decay. The 9MG oxidation rate constants are 4.6×10^7 $M^{-1}\cdot s^{-1}$ at pH 10.0 and 0.12×10^7 $M^{-1}\cdot s^{-1}$ at pH 7.0 for pure 9MG, and 3.6×10^7 $M^{-1}\cdot s^{-1}$ at pH 10.0 and 0.3×10^7 $M^{-1}\cdot s^{-1}$ at pH 7.0 for 9MG + $LysNH_2$. The fact that, within the combined experimental uncertainties, the overall rate constants remain nearly constant regardless of $9MOG^{OX}$–$LysNH_2$ cross-linking supports our interpretation of the reaction PESs. That is, the initial $^1O_2$ addition to 9MG remains as the rate-limiting under all different reaction conditions. All of the downstream steps are exothermic with respect to starting reactants. The C5-cross-linking of $9MOG^{OX}$ with $LysNH_2$ significantly suppressed the formation of 9MSp via C5-water addition. These results have provided a quantitative picture of the formation, structures, and transformations of the C5-water and C5-lysine adducts during the $^1O_2$ oxidation of guanine.

■ ASSOCIATED CONTENT

Supporting Information

The Supporting Information is available free of charge at https://pubs.acs.org/doi/10.1021/acs.jpcb.9b08796.

Calibration of [$^1O_2$] in solution, structures of neutral and protonated $LysNH_2$ tautomers and their Cartesian coordinates, schematic of experimental setup, Cartesian coordinates of structures and images of TSs in Figures 3–5 (PDF)

■ AUTHOR INFORMATION

Corresponding Author

*E-mail: jianbo.liu@qc.cuny.edu; Phone: 1-718-997-3271.

ORCID

Jianbo Liu: 0000-0001-9577-3740

Notes

The authors declare no competing financial interest.

■ ACKNOWLEDGMENTS

This work was supported by the National Science Foundation (Grant no. CHE 1464171) and Queens College Research Enhancement Award. Y.S. and W.L. acknowledge CUNY Mina Rees Doctoral Dissertation Fellowship. W.Z. acknowledges Queens College Trudy Rothman Chemistry Award.

■ REFERENCES

(1) Nonell, S. et al. *Singlet Oxygen: Applications in Biosciences and Nanosciences*; Royal Society of Chemistry, 2016; Vol. *1*, pp 472.

(2) Steenken, S.; Jovanovic, S. V. How Easily Oxidizable Is DNA? One-Electron Reduction Potentials of Adenosine and Guanosine Radicals in Aqueous Solution. *J. Am. Chem. Soc.* **1997**, *119*, 617–618.

(3) Burrows, C. J.; Muller, J. G. Oxidative Nucleobase Modifications Leading to Strand Scission. *Chem. Rev.* **1998**, *98*, 1109–1151.

(4) Zhou, J.; Kostko, O.; Nicolas, C.; Tang, X.; Belau, L.; de Vries, M. S.; Ahmed, M. Experimental Observation of Guanine Tautomers with Vuv Photoionization. *J. Phys. Chem. A* **2009**, *113*, 4829–4832.

(5) Schwell, M.; Hochlaf, M. Photoionization Spectroscopy of Nucleobases and Analogues in the Gas Phase Using Synchrotron Radiation as Excitation Light Source. *Top. Curr. Chem.* **2015**, *355*, 155–208.

(6) Lu, W.; Liu, J. Capturing Transient Endoperoxide in the Singlet Oxygen Oxidation of Guanine. *Chem. Eur. J.* **2016**, *22*, 3127–3138.

(7) Lu, W.; Teng, H.; Liu, J. How Protonation and Deprotonation of 9-Methylguanine Alter Its Singlet O_2 Addition Path: About the Initial Stage of Guanine Nucleoside Oxidation. *Phys. Chem. Chem. Phys.* **2016**, *18*, 15223–15234.

(8) Sun, Y.; Lu, W.; Liu, J. Exploration of the Singlet O_2 Oxidation of 8-Oxoguanine by Guided-Ion Beam Scattering and Density Functional Theory: Changes of Reaction Intermediates, Energetics, and Kinetics Upon Protonation/Deprotonation and Hydration. *J. Phys. Chem. B* **2017**, *121*, 956–966.

(9) Lu, W.; Sun, Y.; Zhou, W.; Liu, J. pH-Dependent Singlet O_2 Oxidation Kinetics of Guanine and 9-Methylguanine: An Online Mass Spectrometry and Spectroscopy Study Combined with Theoretical Exploration. *J. Phys. Chem. B* **2018**, *122*, 40–53.

(10) Sheu, C.; Foote, C. S. Endoperoxide Formation in a Guanosine Derivative. *J. Am. Chem. Soc.* **1993**, *115*, 10446–10447.

(11) Niles, J. C.; Wishnok, J. S.; Tannenbaum, S. R. Spiroiminodihydantoin Is the Major Product of the 8-Oxo-7,8-Dihydroguanosine Reaction with Peroxynitrite in the Presence of Thiols and Guanosine Photooxidation by Methylene Blue. *Org. Lett.* **2001**, *3*, 963–966.

(12) Kang, P.; Foote, C. S. Formation of Transient Intermediates in Low-Temperature Photosensitized Oxidation of an 8-^{13}C-Guanosine Derivative. *J. Am. Chem. Soc.* **2002**, *124*, 4865–4873.

(13) Ye, Y.; Muller, J. G.; Luo, W.; Mayne, C. L.; Shallop, A. J.; Jones, R. A.; Burrows, C. J. Formation of ^{13}C-, ^{15}N-, and ^{18}O–Labeled Guanidinohydantoin from Guanosine Oxidation with Singlet Oxygen. Implications for Structure and Mechanism. *J. Am. Chem. Soc.* **2003**, *125*, 13926–13927.

(14) McCallum, J. E. B.; Kuniyoshi, C. Y.; Foote, C. S. Characterization of 5-Hydroxy-8-Oxo-7,8-Dihydroguanosine in the Photosensitized Oxidation of 8-Oxo-7,8-Dihydroguanosine and Its Rearrangement to Spiroiminodihydantoin. *J. Am. Chem. Soc.* **2004**, *126*, 16777–16782.

(15) Ravanat, J.-L.; Martinez, G. R.; Medeiros, M. H. G.; Di Mascio, P.; Cadet, J. Mechanistic Aspects of the Oxidation of DNA Constituents Mediated by Singlet Molecular Oxygen. *Arch. Biochem. Biophys.* **2004**, *423*, 23–30.

(16) Ravanat, J.-L.; Martinez, G. R.; Medeiros, M. H. G.; Di Mascio, P.; Cadet, J. Singlet Oxygen Oxidation of 2′-Deoxyguanosine. Formation and Mechanistic Insights. *Tetrahedron* **2006**, *62*, 10709–10715.

(17) Lu, W.; Sun, Y.; Tsai, M.; Zhou, W.; Liu, J. Singlet O_2 Oxidation of Deprotonated Guanine-Cytosine Base Pair and Its Entangling with Intra-Base-Pair Proton Transfer. *ChemPhysChem* **2018**, *19*, 2645–2654.

(18) Cadet, J.; Ravanat, J.-L.; Martinez, G. R.; Medeiros, M. H. G.; Di Mascio, P. Singlet Oxygen Oxidation of Isolated and Cellular DNA: Product Formation and Mechanistic Insights. *Photochem. Photobiol.* **2006**, *82*, 1219–1225.

(19) Fleming, A. M.; Burrows, C. J. G-Quadruplex Folds of the Human Telomere Sequence Alter the Site Reactivity and Reaction Pathway of Guanine Oxidation Compared to Duplex DNA. *Chem. Res. Toxicol.* **2013**, *26*, 593–607.

(20) Ravanat, J.-L.; Saint-Pierre, C.; Di Mascio, P.; Martinez, G. R.; Medeiros, M. H. G.; Cadet, J. Damage to Isolated DNA Mediated by Singlet Oxygen. *Helv. Chim. Acta* **2001**, *84*, 3702–3709.

(21) Ravanat, J.-L.; Di Mascio, P.; Martinez, G. R.; Medeiros, M. H. G.; Cadet, J. Singlet Oxygen Induces Oxidation of Cellular DNA. *J. Biol. Chem.* **2000**, *275*, 40601–40604.

(22) Munk, B. H.; Burrows, C. J.; Schlegel, H. B. An Exploration of Mechanisms for the Transformation of 8-Oxoguanine to Guanidinohydantoin and Spiroiminodihydantoin by Density Functional Theory. *J. Am. Chem. Soc.* **2008**, *130*, 5245–5256.

(23) Ye, Y.; Munk, B. H.; Muller, J. G.; Cogbill, A.; Burrows, C. J.; Schlegel, H. B. Mechanistic Aspects of the Formation of Guanidinohydantoin from Spiroiminodihydantoin under Acidic Conditions. *Chem. Res. Toxicol.* **2009**, *22*, 526–535.

(24) Psciuk, B. T.; Schlegel, H. B. Computational Prediction of One-Electron Reduction Potentials and Acid Dissociation Constants for

DOI: 10.1021/acs.jpcb.9b08796
J. Phys. Chem. B 2019, 123, 10410–10423

Guanine Oxidation Intermediates and Products. *J. Phys. Chem. B* **2013**, *117*, 9518−9531.
(25) Grüber, R.; Monari, A.; Dumont, E. Stability of the Guanine Endoperoxide Intermediate: A Computational Challenge for Density Functional Theory. *J. Phys. Chem. A* **2014**, *118*, 11612−11619.
(26) Thapa, B.; Munk, B. H.; Burrows, C. J.; Schlegel, H. B. Computational Study of Oxidation of Guanine by Singlet Oxygen ($^1\Delta_g$) and Formation of Guanine:Lysine Cross-Links. *Chem. - Eur. J.* **2017**, *23*, 5804−5813.
(27) Dumont, E.; Gruber, R.; Bignon, E.; Morell, C.; Moreau, Y.; Monari, A.; Ravanat, J.-L. Probing the Reactivity of Singlet Oxygen with Purines. *Nucleic Acids Res.* **2016**, *44*, 56−62.
(28) Dumont, E.; Gruber, R.; Bignon, E.; Morell, C.; Aranda, J.; Ravanat, J.-L.; Tunon, I. Singlet Oxygen Attack on Guanine: Reactivity and Structural Signature within the B-DNA Helix. *Chem. Eur. J.* **2016**, *22*, 12358−12362.
(29) Iesce, M. R.; Cermola, F.; Temussi, F. Photooxygenation of Heterocycles. *Curr. Org. Chem.* **2005**, *9*, 109−139.
(30) Neeley, W. L.; Essigmann, J. M. Mechanisms of Formation, Genotoxicity, and Mutation of Guanine Oxidation Products. *Chem. Res. Toxicol.* **2006**, *19*, 491−505.
(31) Cadet, J.; Douki, T.; Ravanat, J.-L. Oxidatively Generated Damage to the Guanine Moiety of DNA: Mechanistic Aspects and Formation in Cells. *Acc. Chem. Res.* **2008**, *41*, 1075−1083.
(32) Cadet, J.; Douki, T.; Ravanat, J.-L. Oxidatively Generated Base Damage to Cellular DNA. *Free Radic. Biol. Med.* **2010**, *49*, 9−21.
(33) Fleming, A. M.; Burrows, C. J. Formation and Processing of DNA Damage Substrates for the Hneil Enzymes. *Free Radic. Biol. Med.* **2017**, *107*, 35−52.
(34) Xu, X.; Muller, J. G.; Ye, Y.; Burrows, C. J. DNA-Protein Cross-Links between Guanine and Lysine Depend on the Mechanism of Oxidation for Formation of C5 vs C8 Guanosine Adducts. *J. Am. Chem. Soc.* **2008**, *130*, 703−709.
(35) Solivio, M. J.; Nemera, D. B.; Sallans, L.; Merino, E. J. Biologically Relevant Oxidants Cause Bound Proteins to Readily Oxidatively Cross-Link at Guanine. *Chem. Res. Toxicol.* **2012**, *25*, 326−336.
(36) Morin, B.; Cadet, J. Chemical Aspects of the Benzophenone-Photosensitized Formation of Two Lysine-2′-Deoxyguanosine Cross-Links. *J. Am. Chem. Soc.* **1995**, *117*, 12408−15.
(37) Perrier, S.; Hau, J.; Gasparutto, D.; Cadet, J.; Favier, A.; Ravanat, J.-L. Characterization of Lysine-Guanine Cross-Links Upon One-Electron Oxidation of a Guanine-Containing Oligonucleotide in the Presence of a Trilysine Peptide. *J. Am. Chem. Soc.* **2006**, *128*, 5703−5710.
(38) Jena, N. R.; Mishra, P. C. Interaction of Guanine, Its Anions, and Radicals with Lysine in Different Charge States. *J. Phys. Chem. B* **2007**, *111*, 5418−5424.
(39) Uvaydov, Y.; Geacintov, N. E.; Shafirovich, V. Generation of Guanine-Amino Acid Cross-Links by a Free Radical Combination Mechanism. *Phys. Chem. Chem. Phys.* **2014**, *16*, 11729−11736.
(40) Thapa, B.; Munk, B. H.; Burrows, C. J.; Schlegel, H. B. Computational Study of the Radical Mediated Mechanism of the Formation of C8, C5, and C4 Guanine:Lysine Adducts in the Presence of the Benzophenone Photosensitizer. *Chem. Res. Toxicol.* **2016**, *29*, 1396−1409.
(41) Fleming, A. M.; Armentrout, E. I.; Zhu, J.; Muller, J. G.; Burrows, C. J. Spirodi(Iminohydantoin) Products from Oxidation of 2′-Deoxyguanosine in the Presence of NH_4Cl in Nucleoside and Oligodeoxynucleotide Contexts. *J. Org. Chem.* **2015**, *80*, 711−721.
(42) Thapa, B.; Hebert, S. P.; Munk, B. H.; Burrows, C. J.; Schlegel, H. B. Computational Study of the Formation of C8, C5, and C4 Guanine:Lysine Adducts via Oxidation of Guanine by Sulfate Radical Anion. *J. Phys. Chem. A* **2019**, *123*, 5150−5163.
(43) Bignon, E.; Chan, C.-H.; Morell, C.; Monari, A.; Ravanat, J.-L.; Dumont, E. Molecular Dynamics Insights into Polyamine-DNA Binding Modes: Implications for Crosslink Selectivity. *Chem. − Eur. J.* **2017**, *23*, 12845−12852.
(44) Chan, C.-H.; Monari, A.; Ravanat, J.-L.; Dumont, E. Probing Interaction of a Trilysine Peptide with DNA Behind Formation of Guanine-Lysine Cross-Links: Insights from Molecular Dynamics. *Phys. Chem. Chem. Phys.* **2019**, *21*, 23418−23424.
(45) Freccero, M.; Gandolfi, R.; Sarzi-Amade, M. Selectivity of Purine Alkylation by a Quinone Methide. Kinetic or Thermodynamic Control? *J. Org. Chem.* **2003**, *68*, 6411−6423.
(46) Chin, W.; Mons, M.; Piuzzi, F.; Tardivel, B.; Dimicoli, I.; Gorb, L.; Leszczynski, J. Gas Phase Rotamers of the Nucleobase 9-Methylguanine Enol and Its Monohydrate: Optical Spectroscopy and Quantum Mechanical Calculations. *J. Phys. Chem. A* **2004**, *108*, 8237−8243.
(47) Saigusa, H.; Urashima, S.-h.; Asami, H. IR-UV Double Resonance Spectroscopy of the Hydrated Clusters of Guanosine and 9-Methylguanine: Evidence for Hydration Structures Involving the Sugar Group. *J. Phys. Chem. A* **2009**, *113*, 3455−3462.
(48) Feketeová, L.; Khairallah, G. N.; Chan, B.; Steinmetz, V.; Maître, P.; Radom, L.; O'Hair, R. A. J. Gas-Phase Infrared Spectrum and Acidity of the Radical Cation of 9-Methylguanine. *Chem. Commun.* **2013**, *49*, 7343−7345.
(49) Gonzalez, J.; Banos, I.; Leon, I.; Contreras-Garcia, J.; Cocinero, E. J.; Lesarri, A.; Fernandez, J. A.; Millan, J. Unravelling Protein-DNA Interactions at Molecular Level: A DFT and NCI Study. *J. Chem. Theory Comput.* **2016**, *12*, 523−534.
(50) Song, B.; Zhao, J.; Griesser, R.; Meiser, C.; Sigel, H.; Lippert, B. Effects of (N7)-Coordinated Nickel(II), Copper(II), or Platinum(II) on the Acid-Base Properties of Guanine Derivatives and Other Related Purines. *Chem. Eur. J.* **1999**, *5*, 2374−2387.
(51) Blackburn, G. M.; Gait, M. J.; Loakes, D.; Williams, D. M. *Nucleic Acids in Chemistry and Biology*; Royal Society of Chemistry: Cambridge, UK, 2006.
(52) Domínguez-Martín, A.; Johannsen, S.; Sigel, A.; Operschall, B. P.; Song, B.; Sigel, H.; Okruszek, A.; González-Pérez, J. M.; Niclós-Gutiérrez, J.; Sigel, R. K. O. Intrinsic Acid-Base Properties of a Hexa-2′-Deoxynucleoside Pentaphosphate, D(ApGpGpCpCpT): Neighboring Effects and Isomeric Equilibria. *Chem. Eur. J.* **2013**, *19*, 8163−8181.
(53) Velikyan, I.; Acharya, S.; Trifonova, A.; Foeldesi, A.; Chattopadhyaya, J. The pKa's of 2′-Hydroxyl Group in Nucleosides and Nucleotides. *J. Am. Chem. Soc.* **2001**, *123*, 2893−2894.
(54) Midey, A.; Dotan, I.; Viggiano, A. A. Temperature Dependences for the Reactions of O^- and O_2^- with $O_2(a^1\Delta_g)$ from 200 to 700 K. *J. Phys. Chem. A* **2008**, *112*, 3040−3045.
(55) Fang, Y.; Liu, F.; Bennett, A.; Ara, S.; Liu, J. Experimental and Trajectory Study on Reaction of Protonated Methionine with Electronically Excited Singlet Molecular Oxygen ($a^1\Delta_g$): Reaction Dynamics and Collision Energy Effects. *J. Phys. Chem. B* **2011**, *115*, 2671−2682.
(56) Lafferty, W. J.; Solodov, A. M.; Lugez, C. L.; Fraser, G. T. Rotational Line Strengths and Self-Pressure-Broadening Coefficients for the 1.27 μm, $a^1\Delta_g$-$X^3\sum_g^-$, ν = 0-0 Band of O_2. *Appl. Opt.* **1998**, *37*, 2264−2270.
(57) Liu, F.; Lu, W.; Yin, X.; Liu, J. Mechnistic and Kinetic Study of Singlet O_2 Oxidation of Methionine by On-Line Electrospray Ionization Mass Spectrometry. *J. Am. Soc. Mass Spectrom.* **2016**, *27*, 59−72.
(58) Mark, L. P.; Gill, M. C.; Mahut, M.; Derrick, P. J. Dual Nano-Electrospray for Probing Solution Interactions and Fast Reactions of Complex Biomolecules. *Eur. J. Mass Spectrom.* **2012**, *18*, 439−466.
(59) Fisher, C. M.; Kharlamova, A.; McLuckey, S. A. Affecting Protein Charge State Distributions in Nano-Electrospray Ionization Via in-Spray Solution Mixing Using Theta Capillaries. *Anal. Chem.* **2014**, *86*, 4581−4588.
(60) Mortensen, D. N.; Williams, E. R. Theta-Glass Capillaries in Electrospray Ionization: Rapid Mixing and Short Droplet Lifetimes. *Anal. Chem.* **2014**, *86*, 9315−9321.
(61) Wampler, F. M.; Blades, A. T.; Kebarle, P. Negative Ion Electrospray Mass Spectrometry of Nucleotides: Ionization from

DOI: 10.1021/acs.jpcb.9b08796
J. Phys. Chem. B 2019, 123, 10410−10423

Water Solution with SF_6 Discharge Suppression. *J. Am. Soc. Mass Spectrom.* **1993**, *4*, 289−295.
(62) Fang, Y.; Liu, J. Reaction of Protonated Tyrosine with Electronically Excited Singlet Molecular Oxygen ($a^1\Delta_g$): An Experimental and Trajectory Study. *J. Phys. Chem. A* **2009**, *113*, 11250−11261.
(63) Petersson, G. A.; Al-Laham, M. A. A Complete Basis Set Model Chemistry. Ii. Open-Shell Systems and the Total Energies of the First-Row Atoms. *J. Chem. Phys.* **1991**, *94*, 6081−90.
(64) Marenich, A. V.; Cramer, C. J.; Truhlar, D. G. Universal Solvation Model Based on Solute Electron Density and on a Continuum Model of the Solvent Defined by the Bulk Dielectric Constant and Atomic Surface Tensions. *J. Phys. Chem. B* **2009**, *113*, 6378−6396.
(65) Chai, J.-D.; Head-Gordon, M. Long-Range Corrected Hybrid Density Functionals with Damped Atom−Atom Dispersion Corrections. *Phys. Chem. Chem. Phys.* **2008**, *10*, 6615−6620.
(66) Frisch, M. J.; Trucks, G. W.; Schlegel, H. B.; Scuseria, G. E.; Robb, M. A.; Cheeseman, J. R.; Scalmani, G.; Barone, V.; Mennucci, B.; Petersson, G. A.; et al. *Gaussian 09*, revision D.01; Gaussian, Inc: Wallingford, CT, 2013.
(67) Alecu, I. M.; Zheng, J.; Zhao, Y.; Truhlar, D. G. Computational Thermochemistry: Scale Factor Databases and Scale Factors for Vibrational Frequencies Obtained from Electronic Model Chemistries. *J. Chem. Theory Comput.* **2010**, *6*, 2872−2887.
(68) Leng, Y.; Zhang, M.; Song, C.; Chen, M.; Lin, Z. A Semi-Empirical and Ab-Initio Combined Approach for the Full Conformational Searches of Gaseous Lysine and Lysine-H_2O Complex. *J. Mol. Struct.: THEOCHEM* **2008**, *858*, 52−65.
(69) Boeckx, B.; Maes, G. Experimental and Theoretical Observation of Different Intramolecular H-Bonds in Lysine Conformations. *J. Phys. Chem. B* **2012**, *116*, 12441−12449.
(70) Voet, D.; Voet, J. G.; Pratt, C. W. *Fundamentals Biochemistry*; John Wiley & Sons, Inc.: Hoboken, NJ, 2002.
(71) J. A., Riddick; Bunger, W. B.; Sakano, T. K. *Techniques of Chemistry; V. II. Organic Solvents: Physical Properties and Methods of Purification*, 4th ed.; Wiley: New York, 1986; Vol. *II*, pp p655.
(72) Kemnitz, C. R.; Loewen, M. J. "Amide Resonance" Correlates with a Breadth of C−N Rotation Barriers. *J. Am. Chem. Soc.* **2007**, *129*, 2521−2528.
(73) Lu, W.; Liu, F.; Emre, R.; Liu, J. Collision Dynamics of Protonated N-Acetyl Methionine with Singlet Molecular Oxygen ($a^1\Delta_g$): The Influence of Amide Bond and Ruling out the Complex-Mediated Mechanism at Low Energies. *J. Phys. Chem. B* **2014**, *118*, 3844−3852.
(74) Maranzana, A.; Ghigo, G.; Tonachini, G. Diradical and Peroxirane Pathways in the [Π2 + Π2] Cycloaddition Reactions of $^1\Delta_g$ Dioxygen with Ethene, Methyl Vinyl Ether, and Butadiene: A Density Functional and Multireference Perturbation Theory Study. *J. Am. Chem. Soc.* **2000**, *122*, 1414−1423.
(75) Lee, T. J.; Taylor, P. R. A Diagnostic for Determining the Quality of Single-Reference Electron Correlation Methods. *Int. J. Quantum Chem.* **1989**, *36*, 199−207.
(76) Saito, T.; Nishihara, S.; Kataoka, Y.; Nakanishi, Y.; Matsui, T.; Kitagawa, Y.; Kawakami, T.; Okumura, M.; Yamaguchi, K. Transition State Optimization Based on Approximate Spin-Projection (AP) Method. *Chem. Phys. Lett.* **2009**, *483*, 168−171.
(77) Saito, T.; Nishihara, S.; Kataoka, Y.; Nakanishi, Y.; Kitagawa, Y.; Kawakami, T.; Yamanaka, S.; Okumura, M.; Yamaguchi, K. Reinvestigation of the Reaction of Ethylene and Singlet Oxygen by the Approximate Spin Projection Method. Comparison with Multireference Coupled-Cluster Calculations. *J. Phys. Chem. A* **2010**, *114*, 7967−7974.
(78) Woon, D. E.; Dunning, T. H., Jr. Gaussian Basis Sets for Use in Correlated Molecular Calculations. III. The Atoms Aluminum through Argon. *J. Chem. Phys.* **1993**, *98*, 1358−71.
(79) Alshykhly, O. R.; Fleming, A. M.; Burrows, C. J. 5-Carboxamido-5-Formamido-2-Iminohydantoin, in Addition to 8-Oxo-7,8-Dihydroguanine, Is the Major Product of the Iron-Fenton or x-Ray Radiation-Induced Oxidation of Guanine under Aerobic Reducing Conditions in Nucleoside and DNA Contexts. *J. Org. Chem.* **2015**, *80*, 6996−7007.
(80) Morin, B.; Cadet, J. Type I Benzophenone-Mediated Nucleophilic Reaction of 5′-Amino-2′,5′-Dideoxyguanosine. A Model System for the Investigation of Photosensitized Formation of DNA-Protein Cross-Links. *Chem. Res. Toxicol.* **1995**, *8*, 792−9.
(81) Lu, W.; Liu, F.; Emre, R.; Liu, J. Collision Dynamics of Protonated N-Acetylmethionine with Singlet Molecular Oxygen ($a^1\Delta_g$): The Influence of the Amide Bond and Ruling out the Complex-Mediated Mechanism at Low Energies. *J. Phys. Chem. B* **2014**, *118*, 3844−3852.

DOI: 10.1021/acs.jpcb.9b08796
J. Phys. Chem. B 2019, 123, 10410−10423